ATF4-dependent induction of heme oxygenase 1 prevents anoikis and promotes metastasis

Souvik Dey,[1] Carly M. Sayers,[2] Ioannis I. Verginadis,[1] Stacey L. Lehman,[1] Yi Cheng,[1] George J. Cerniglia,[1] Stephen W. Tuttle,[1] Michael D. Feldman,[3] Paul J.L. Zhang,[3] Serge Y. Fuchs,[4] J. Alan Diehl,[5] and Constantinos Koumenis[1]

[1]Department of Radiation Oncology, Perelman School of Medicine, [2]Graduate Program in Pharmacology, Biomedical Graduate School, and [3]Department of Pathology and Laboratory Medicine, Perelman School of Medicine, University of Pennsylvania, Philadelphia, Pennsylvania, USA. [4]Department of Animal Biology and Mari Lowe Center for Comparative Oncology, School of Veterinary Medicine, University of Pennsylvania, Philadelphia, Pennsylvania, USA. [5]Department of Biochemistry and Molecular Biology, Hollings Cancer Center, Medical University of South Carolina, Charleston, South Carolina, USA.

The integrated stress response (ISR) is a critical mediator of cancer cell survival, and targeting the ISR inhibits tumor progression. Here, we have shown that activating transcription factor 4 (ATF4), a master transcriptional effector of the ISR, protects transformed cells against anoikis — a specialized form of apoptosis — following matrix detachment and also contributes to tumor metastatic properties. Upon loss of attachment, ATF4 activated a coordinated program of cytoprotective autophagy and antioxidant responses, including induced expression of the major antioxidant enzyme heme oxygenase 1 (HO-1). HO-1 upregulation was the result of simultaneous activation of ATF4 and the transcription factor NRF2, which converged on the *HO1* promoter. Increased levels of HO-1 ameliorated oxidative stress and cell death. ATF4-deficient human fibrosarcoma cells were unable to colonize the lungs in a murine model, and reconstitution of ATF4 or HO-1 expression in ATF4-deficient cells blocked anoikis and rescued tumor lung colonization. HO-1 expression was higher in human primary and metastatic tumors compared with noncancerous tissue. Moreover, HO-1 expression correlated with reduced overall survival of patients with lung adenocarcinoma and glioblastoma. These results establish HO-1 as a mediator of ATF4-dependent anoikis resistance and tumor metastasis and suggest ATF4 and HO-1 as potential targets for therapeutic intervention in solid tumors.

Introduction

Over the course of tumor development, cancer cells encounter various microenvironmental stresses, including hypoxia and nutrient deprivation (1). In response to these stress conditions, cells activate a number of homeostatic pathways that are collectively known as the integrated stress response (ISR). Activation of ISR is accompanied by a global reduction of protein synthesis caused by phosphorylation of translation initiation factor eIF2α by a family of eIF2 kinases that includes PERK and GCN2 (2–4). Paradoxically, the increase in eIF2α phosphorylation leads to enhanced expression of activating transcription factor 4 (ATF4), a basic leucine zipper (bZIP) transcription factor (5), primarily via enhanced translation of its mRNA by a mechanism involving its 5′ UTR (6). ATF4 in turn transcriptionally upregulates multiple effectors that ultimately determine cell fate, depending on the severity and duration of the stress as well as other microenvironmental factors. Tumor cells have been shown to induce ISR to adapt to physiological stress conditions in their microenvironment, such as hypoxia and nutrient deprivation (7–9).

Failure to fully induce ISR by eIF2 kinases PERK and GCN2 and to activate ATF4 reduces tumor cell growth in vitro and in vivo (10–12). Human tumor samples exhibit higher levels of ATF4 compared with corresponding normal tissues, and ATF4 expression overlaps with areas of hypoxia in human cervical carcinomas (10), supporting a prosurvival role for ATF4 in these conditions. Moreover, deletion or knockdown of ATF4 from transformed cells results in significantly reduced tumor growth in a xenograft model (11). Interestingly, ATF4 overexpression correlates with resistance to chemotherapeutic agents, including cisplatin, doxorubicin, vincristine, and etoposide (13–15).

More recently, deletion of *Perk* in a mouse model of mammary carcinoma was reported to reduce the incidence of tumor metastasis (12). Since ATF4 is downstream of PERK, it could also play a role in the metastatic cascade. Inhibition of PERK or knockdown of GCN2 decreases the migration of breast cancer and melanoma cells in in vitro assays (16). Additionally, ATF4 was shown to be a crucial regulator of the epithelial-to-mesenchymal transition (EMT) in neural crest cells, a process that is required for metastasis of epithelial tumors (17).

Loss of attachment of cancer cells to the extracellular matrix (ECM) is required for them to intravasate and enter into the blood and lymphatic vessels (18). While in circulation, the cancer cells must then survive the hostile environment of the circulation and resist anoikis, which is a specialized form of cell death caused by loss of contact with the ECM (19, 20). Metastatic cancer cells have been shown to develop resistance to anoikis by activating several signaling pathways that impinge on extrinsic and mitochondria-mediated apoptosis (20, 21).

PERK-mediated activation of the ISR following matrix detachment in mammary epithelial cells (MECs) was shown to promote survival and is required for proper luminal filling in 3D cultures

Authorship note: Souvik Dey and Carly M. Sayers have contributed equally to this work.
Conflict of interest: The authors have declared that no conflict of interest exists.
Submitted: July 16, 2014; **Accepted:** April 17, 2015.
Reference information: *J Clin Invest*. 2015;125(7):2592–2608. doi:10.1172/JCI78031.

and lactating mammary glands in vivo (22). However, the precise role of ATF4 in these processes as well as the mechanistic basis for such a role has not been elucidated. Here, we have focused on the specific role that ATF4 plays in metastatic behavior, including migration, invasion, and the ability to colonize distant sites. We found that the ISR is robustly activated following loss of matrix attachment and acts as a prosurvival signal by inducing an ATF4-dependent cytoprotective autophagic response characterized by transcriptional regulation of key autophagy genes, such as *ATG5*, *ATG7*, and *ULK1*. Furthermore, we show that ATF4 dramatically reduced ROS production to prevent anoikis. Activation of the antioxidant response is characterized by increased expression of several antioxidant genes, particularly heme oxygenase 1 (HO-1), a rate-limiting enzyme that degrades heme to carbon monoxide (CO), biliverdin, and ferrous iron (23). Intriguingly, induction of HO-1 is dependent upon NRF2, a master antioxidant transcription factor that is also regulated by PERK (23–26). Finally, we also demonstrate that the ATF4-dependent, prosurvival response is critical for effective lung colonization in mice and that HO-1 expression is a predictive marker for reduced overall survival in lung cancer and glioblastoma patients. Taken together, our studies indicate that ATF4 plays a central role in mediating an antioxidant and pro-autophagic ISR that enables cancer cells to survive and migrate to secondary sites during tumor metastasis.

Results

Effect of ATF4 expression on tumor cell migration and invasion. Invasion and migration are key cellular attributes necessary for metastasis, and depletion of ATF4 has been implicated in decreasing cell migration during hypoxia (16). To examine the effect of ATF4 expression on the migration of HT1080 human fibrosarcoma cells (a cell line shown to form aggressive metastatic tumors in mouse lungs), we utilized scratch and Transwell migration assays. When HT1080 cells stably expressing either a nontargeting shRNA (shNT.HT1080) or an shRNA against ATF4 (shATF4.HT1080) were tested with the scratch assay under normoxia, no difference was seen in the rate of scratch closure between the 2 cell lines (Supplemental Figure 1A; supplemental material available online with this article; doi:10.1172/JCI78031DS1). Next, we assessed the migratory ability of shNT.HT1080 and shATF4 cells under hypoxia (0.5%) by Transwell migration. shNT and shATF4.HT1080 cells were exposed to either 0.5 % hypoxia followed by normoxia for 10 hours (Supplemental Figure 1B) or to hypoxia alone (Supplemental Figure 1C). No significant differences in the migratory behavior of ATF4-replete or -deficient cells were observed (Supplemental Figure 1, B and C). To determine whether ATF4 affects cell invasion, HT1080 cells with or without ATF4 (shNT and shATF4) were plated in 24 Transwell Matrigel–coated plates and cell invasion was assayed after exposed with hypoxia (0.5%) for 8 hours. As with the migration assay above, ATF4 expression did not significantly alter the invasive capability of the HT1080 cells (Supplemental Figure 1D).

Matrix detachment induces the ISR and the unfolded protein response. Metastasis also requires detachment of tumor cells from the ECM, intravasation, and transport via the bloodstream to their secondary location. Loss of ECM attachment in epithelial cells has been reported to induce PERK-mediated stress response (22). To test this, we subjected HT1080 cells to suspension stress. Increased eIF2α phosphorylation (p-eIF2α) was detected in cells under suspension compared with the cells grown in attachment conditions (Figure 1A) at 24 hours and was sustained for 36 hours. Levels of p-eIF2α following ECM loss were comparable to levels in those cells that were treated with thapsigargin (TG), a SERCA pump inhibitor and well-established inducer of ISR. A concomitant increase in ATF4 levels was also detected (Figure 1A). A similar induction of ISR through PERK was also observed in DLD1 colorectal adenocarcinoma cells (Supplemental Figure 2), demonstrating that this effect was not restricted to a single cell type. A significant upregulation of the mRNA levels of the ATF4 transcriptional targets DNA damage–inducible transcript-3 (*DDIT3/CHOP*), *ATF3*, and asparagine synthetase (*ASNS*) after 48 hours indicated an effective induction of the ISR by ATF4 (Figure 1B). These results demonstrate that loss of ECM attachment stimulates ISR signaling characterized by induction of ATF4 and its target genes.

PERK-mediated eIF2α phosphorylation is one of the 3 signaling pathways activated during the unfolded protein response (UPR) (27). The other signaling modules consist of splicing and enhanced translation of the transcription factor XBP1 by the endonuclease/kinase IRE1α and translocation and proteolytic cleavage of the transcription factor ATF6. Loss of matrix attachment for 48 hours in HT1080 cells resulted in a robust increase of spliced *XBP1* transcript and XBP1s protein expression (Supplemental Figure 3, A and B). We also detected an increase in ATF6 processing by 24 hours that was sustained until 48 hours (Supplemental Figure 3B). Levels of XBP1s and cleaved ATF6 protein were comparable to those induced by TG, indicating that the full spectrum of UPR responses was elicited following detachment stress.

Loss of ISR signaling increases anoikis-mediated cell death. Loss of matrix attachment leads to programmed cell death — a phenomenon known as anoikis (20). During the 48-hour period following detachment, we did not observe significant levels of apoptosis, as characterized by the absence of cleaved PARP (c-PARP) and c–caspase 3 in HT1080 or DLD1 cells (Figure 1A and Supplemental Figure 2). In contrast, the proapoptotic agent staurosporine (ST) caused a substantial increase in apoptosis markers in these cells.

The ISR can have differential effects on cellular fate (both survival and death), depending on the duration, severity and nature of the stress. To determine the role of ISR in cell fate, HT1080 cells stably transfected with either shNT or shRNA against PERK (shPERK) were subjected to suspension conditions. Compared with the induction of ATF4 expression and eIF2α phosphorylation in shNT.HT1080 cells, induction of eIF2α phosphorylation and ATF4 expression were significantly attenuated in shPERK.HT1080 cells, which also exhibited significantly increased levels of c-PARP and c–caspase 3 (Figure 1C), corresponding to a 2-fold reduction in surviving cell fraction of shPERK.HT1080 cells by 48 hours (Figure 1E).

As an alternate approach to blocking PERK activation under these conditions, we utilized a highly specific PERK inhibitor (GSK414) that binds to kinase domain and inhibits PERK activity (28). Treatment of HT1080 cells (Figure1D) or DLD1 cells (Supplemental Figure 2) with GSK414 blocked PERK activation in suspension cultures, as evident from reduced p-PERK levels, p-eIF2α

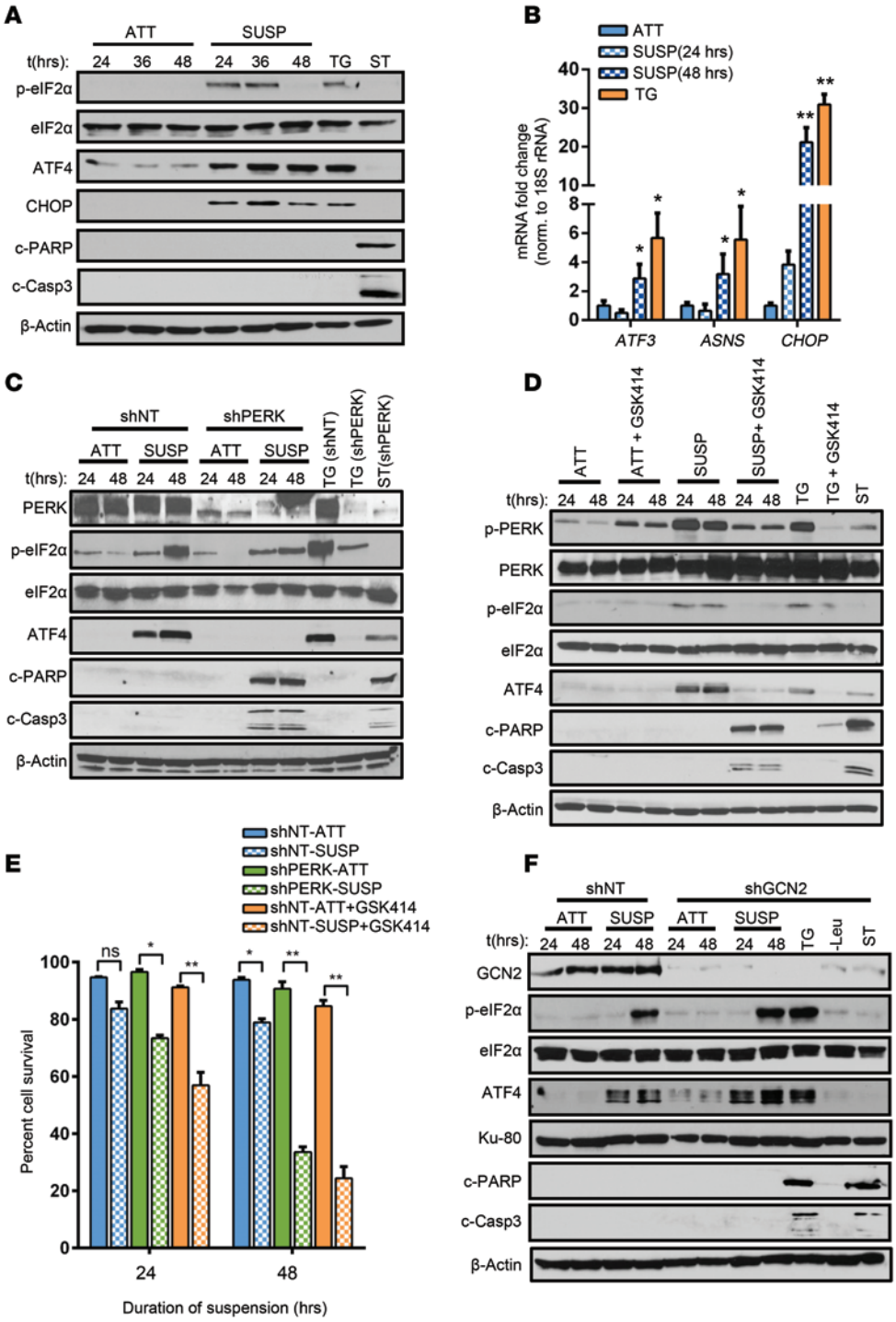

Figure 1. Induction of the ISR is critical for resistance to anoikis. (**A**) HT1080 cells were grown in attached (ATT) or suspension (SUSP) conditions and treated with 0.5 μM TG or with 1 μM ST. Whole-cell lysates were used to detect levels of p-eIF2α, eIF2α, ATF4, CHOP, c-PARP, cleaved caspase-3 (c-Casp3), and β-actin. (**B**) Transcript levels of *CHOP*, *ATF3*, and *ASNS* relative to 18S rRNA. Data are represented as mean fold change compared with attached cultures for 3 independent experiments (n = 3, mean ± SD). *$P < 0.05$; **$P < 0.01$, Student's t test. (**C**) HT080 cells transfected with shNT or shPERK were cultured in attached or suspension conditions, and Western blot analysis was performed. (**D**) shNT. HT1080 cells were treated with 1 μM PERK inhibitor GSK2606414 (GSK414) in attached or in suspension culture. Immunoblot analysis for the indicated proteins was performed. (**E**) Cell viability was analyzed by Trypan blue exclusion assay and is represented as the mean percentage cell survival of 3 independent experiments (n = 3, mean ± SD). *$P < 0.01$; **$P < 0.001$, by Student's t test. (**F**) HT1080 stably transfected with shRNA against GCN2 (shGCN2) and nontargeting counterpart (shNT) were cultured in attached and suspension conditions and immunoblotted for the indicated proteins. All immunoblots are representative of 2 independent experiments.

levels, and ATF4 induction (Figure 1D and Supplemental Figure 2). While GSK414 alone did not cause any significant increase in apoptosis in attached cells, treatment of suspension cultures resulted in significant induction of c-PARP and c–caspase 3 levels, which corresponded to about 70% reduction in cellular survival by 48 hours (Figure 1E). To investigate whether the cytoplasmic, amino acid–sensing kinase GCN2 played any role in conferring anoikis resistance, we also subjected shGCN2.HT1080 cells to attached and suspension conditions. Absence of GCN2 did not cause any change in elevated p-eIF2α or ATF4 levels by 48 hours of suspension stress (Figure 1F). Moreover, shGCN2.HT1080 cells did not display any significant induction of apoptosis markers, indicating that GCN2 does not play a causative role in resistance to anoikis. We conclude from these results that induction of PERK following cellular matrix detachment is a mechanism to resist anoikis-mediated cell death.

ATF4 plays a critical role in resistance to anoikis. We wanted to determine the role of ATF4 in providing resistance to anoikis. Both shNT.HT1080 and shNT.DLD1 cells exhibited ATF4 induction following matrix detachment (Figure 2, A and B). In contrast, knock-

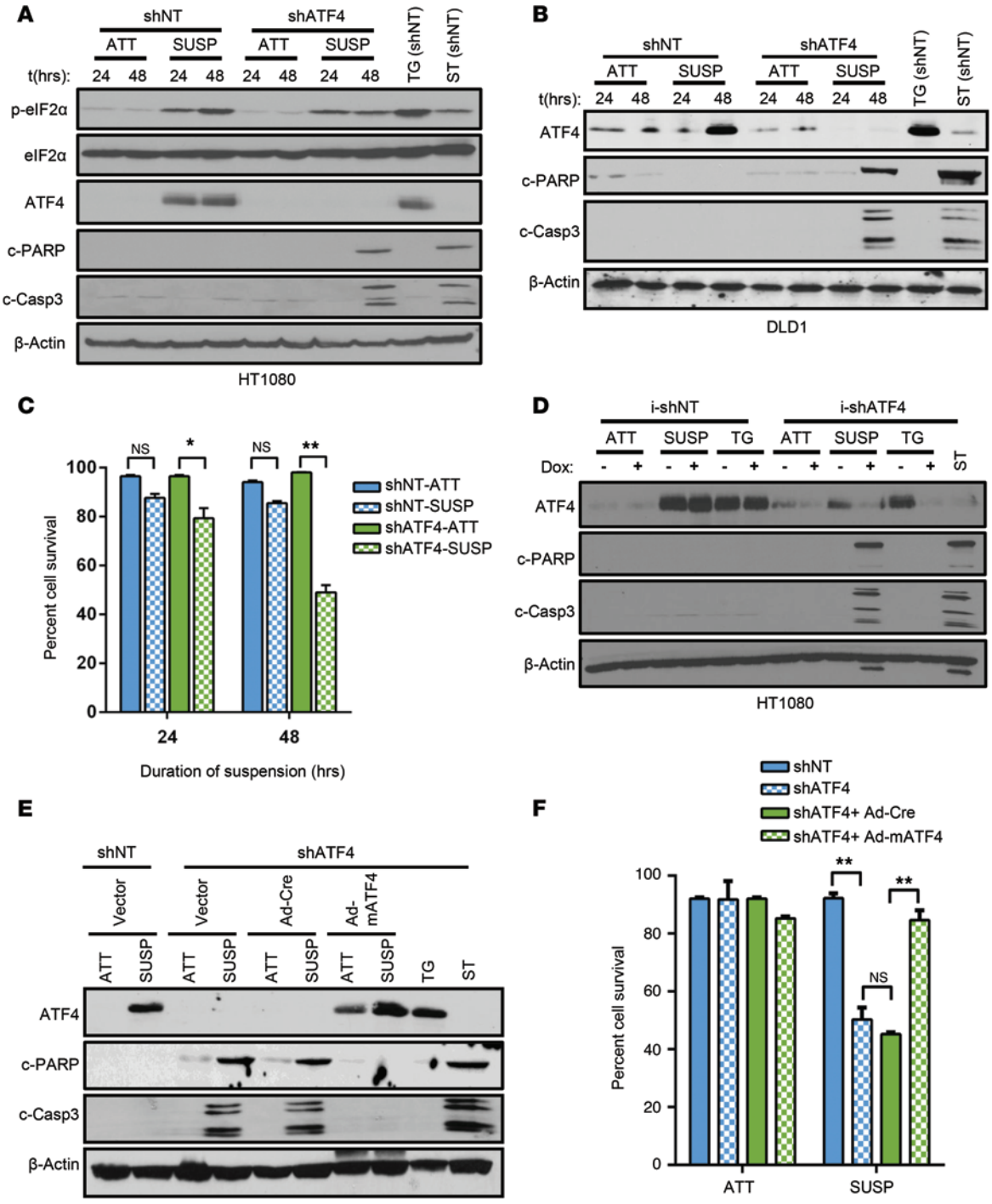

Figure 2. ATF4 confers resistance to anoikis. shNT and shATF4.HT1080 (**A**) as well as shNT and shATF4.DLD1 cells (**B**) were grown in attached or in suspension conditions, and Western blot analysis for markers of the ISR and apoptosis was performed. (**C**) Mean percentage cell viability from 3 independent experiments was measured in shNT and shATF4.HT1080 cells grown in suspension (n = 3, mean ± SD). *P < 0.05; **P < 0.01, Student's t test. (**D**) HT1080 cells stably expressing tetracycline i-shATF4 or i-shNT were grown in attached or suspension conditions for 48 hours or treated with 0.5 μM TG after pretreatment either with DMSO (–) or Dox (+) to alter ATF4 expression. Levels of c-PARP and cleaved caspase-3 were measured and compared with ST treatment. (**E**) Immunoblots of lysates from shATF4.HT1080 infected with empty vector, control (Ad-Cre), or mATF4 (Ad-mATF4) and grown in attached or suspension cultures for 48 hours. (**F**) Cell viability by Trypan blue exclusion assay. Percentage of cell survival is represented as mean ± SD from 3 independent experiments (n = 3, mean ± SD). *P < 0.05; **P < 0.01, Student's t test. All immunoblots are representative of 2 independent experiments.

down of ATF4 expression by stably transfecting shRNA (shATF4) in both cell lines resulted in higher levels of apoptosis, corresponding to over 50% reduction of cell survival (Figure 2, A–C). Additionally, we utilized the CRISPR/CAS9 system to target the exon 2 of the *ATF4*-coding sequence and developed a CRISPR-ATF4 HT1080 cell line. Similarly to shATF4.HT1080 cells, CRISPR-ATF4.HT1080 cells demonstrated increased sensitivity to anoikis following 48 hours of suspension (Supplemental Figure 4A). Compared with shPERK cells, for which 24 hours of suspension was sufficient for induction of apoptosis, we did not observe significant anoikis in shATF4.HT1080 or in CRISPR-ATF4 HT1080 cells until 48 hours in suspension (Figure 2A and Supplemental Figure 4A). This delay could be attributed to other cellular effects of PERK, independent of ATF4 activation, such as downregulation of IFN signaling and activation of NRF2 (29, 30).

To further probe the role of ATF4 in resistance to anoikis, we developed a HT1080 cell line in which the levels of ATF4 could be modulated by a doxycycline-inducible (Dox-inducible) shRNA against ATF4 (i-shATF4). This system permitted regulated expression of ATF4 without direct modulation of any other component of the ISR. Addition of Dox effectively blocked the expression of ATF4 following TG treatment as well as in suspension conditions (Figure 2D). Importantly, Dox treatment of i-shATF4.HT1080 cells resulted in a significant increase in apoptosis compared with treatment of i-shNT.HT1080 cells (Figure 2D). To minimize the possibility that the effects seen with the shATF4 cells were due to off-target effects of the shRNA, a full-length version of mouse ATF4 (mATF4) was expressed using adenovirus-mediated transduction in shATF4.HT1080 cells (Figure 2E). As a control, we also infected shATF4 cells with adeno-Cre to rule out any effects that could be induced by viral infection. In contrast to adeno-Cre–infected shATF4.HT1080 cells, expression of mATF4 in shATF4.HT1080 cells completely blocked anoikis, with no significant reduction in the percentage of surviving cells following suspension stress (Figure 2, E and F). Finally, we tested to determine whether expressing ATF4 in *trans* could rescue cells from anoikis in the absence of PERK. Expression of mATF4 in shPERK.HT1080 did not reverse the anoikis-sensitive phenotype, further supporting an essential role of PERK and additional signaling in this process (Supplemental Figure 3B).

ATF4-dependent cytoprotective autophagy decreases anoikis. Matrix detachment has been shown to induce a PERK-dependent autophagy program to survive anoikis (22). We wished to determine whether ATF4 plays a critical role in the process. When placed under suspension, HT1080 cells showed induction of autophagy, as evident from processing of LC3BI to LC3BII and degradation of p62 (also referred to as SQSTM1), which acts as a ubiquitin-binding scaffold protein (Figure 3A). In contrast, shATF4.HT1080 cells showed a significant drop in LC3B processing compared with shNT.HT1080 cells in suspension culture by 24 hours (Figure 3B). By 48 hours, the shATF4 cells lacked any LC3BII expression, suggesting that ATF4 expression is critical for autophagy (Figure 3B). Autophagy flux assays that were performed by treating shATF4.HT1080 cells with proteasome inhibitors E64d/Pep revealed reduced LC3B processing compared with shNT.HT1080 cells in suspension (Figure 3C). Importantly, the autophagic response, which could not be sustained in shATF4.HT1080 cells, was recovered when ATF4 expression was reconstituted in *trans* by Ad-mATF4 (Figure 3D).

Autophagy can have both cytoprotective and cytostatic roles toward tumor cells (31). On the one hand, autophagy can suppress tumor cell growth by eliminating unfolded proteins and damaged cellular organelles, particularly during tumor initiation. However, it can also promote tumor cell growth by raising the apoptotic threshold of cells under stress conditions associated with the tumor microenvironment (32). To investigate the role of ATF4-dependent autophagy during loss of ECM attachment, we treated HT1080 cells with increasing concentrations of spautin-1, an autophagy inhibitor that acts by inhibiting the VPS34/PI3K complex required for autophagic vesicle nucleation (33). Spautin-1 treatment (5 and 10 μM) decreased LC3B processing in both attached and suspension culture conditions in HT1080 cells (Figure 3E). Importantly, cells treated with spautin-1 under suspension conditions had significantly increased levels of c-PARP and c–caspase 3 (Figure 3E). Time-course analysis with 5 μM spautin-1 showed significantly increased apoptosis (Figure 3F) and reduced survival (Figure 3G) as early as 24 hours following treatment.

ATF4 transcriptionally modulates several autophagy genes by directly binding to their promoter in response to cellular stress conditions such as hypoxia (34–36). We investigated to determine whether key ATF4-targeted autophagy genes were modulated following matrix detachment. We found a significant increase (~4-fold) in transcript levels as well as protein levels of *ATG5*, *ATG7*, and *ULK1* by 48 hours of suspension (Figure 3H). The expression of these transcripts as well as their corresponding protein levels was dependent on ATF4, as their induction was significantly blocked in its absence (Supplemental Figure 5A). Knockdown of ATG5, ATG7 and ULK1 by siRNA in HT1080 led to abrogated LC3 processing compared with nontargeting siRNA–transfected (siNT-transfected) cells (Supplemental Figure 5, B and C). Similar to our previous observations, failure to induce autophagy in the absence of ATG5, ATG7 or ULK1 led to an increase in apoptosis (Supplemental Figure 5, B and C). Therefore, ATF4-mediated induction of autophagy in response to matrix detachment acts as a cytoprotection mechanism against anoikis.

Loss of ATF4 increases ROS levels in suspension cell cultures. Matrix detachment is often associated with substantial levels of oxidative stress caused by increase in ROS production (37). Interestingly, ATF4 activation has also been linked to cells' protection from oxidative stress, which transcriptionally activates multiple antioxidant genes to maintain redox status in the cells (2, 38). Therefore, we hypothesized that loss of ATF4 should significantly compromise the ability of the cells to ameliorate increased ROS production and should render cells sensitive to anoikis-mediated cell death. To test this, shNT and shATF4.HT1080 cells were treated with vehicle or Trolox, a water-soluble analog of vitamin E and a potent antioxidant, during attached and suspension culture conditions. Addition of Trolox resulted in a significant increase of cell viability of shATF4 cells compared with vehicle-treated cells (Figure 4B). By comparison, Trolox treatment drastically reduced c-PARP and c–caspase 3 levels in suspension of shATF4.HT1080 cells without significantly altering the levels of PERK and eIF2α phosphorylation status (Figure 4A). Coincidentally, activation of anoikis is also associated with glucose deprivation as well as a drop

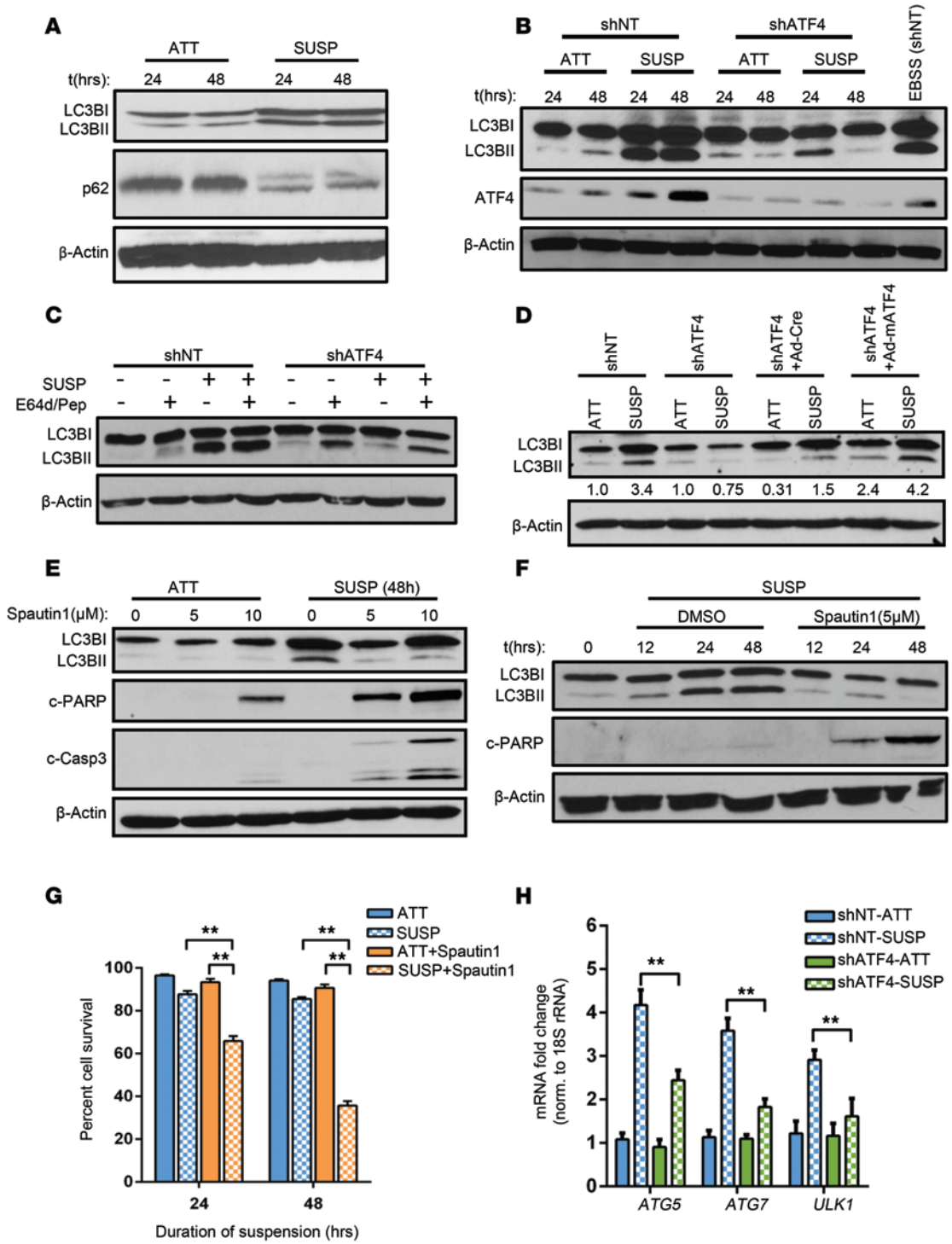

Figure 3. ATF4-mediated autophagy provides cytoprotection against anoikis. (**A**) Levels of autophagy in HT1080 cells grown in attached or suspension conditions were measured by immunoblotting with antibodies against LC3B (LC3BI and LC3BII) and p62. (**B**) Differences in autophagy induction between shNT and shATF4.HT1080 cells in suspension were similarly measured and compared with cells incubated with media devoid of serum (EBSS). (**C**) Autophagy flux assay was performed by treating cells with E-64d (10 μg/ml) and 10 μg/ml pepstatin A (Pep) grown in suspension cultures for 48 hours. (**D**) Immunoblots for LC3B in shNT and shATF4.HT1080 cells transfected with either control (shATF4 + Ad-Cre) or with mATF4 (shATF4 + Ad-mATF4). Ratio of LC3BII to LC3BI is represented as normalized to the attached condition of shNT and shATF4.HT1080 cells. (**E**) Autophagy was inhibited with increasing concentration of spautin-1, and cell lysates were analyzed by Western blots. (**F**) HT1080 cells were treated with spautin-1 (5 μM) for indicated time points. Immunoblots for autophagy and apoptosis markers were similarly performed. All immunoblots are representative of 2 independent experiments. (**G**) Mean cell survival from 3 independent experiments was measured and represented (n = 3, mean ± SD). $^{**}P < 0.01$, Student's t test. (**H**) mRNA levels for *ATG5*, *ATG7*, and *ULK1* relative to 18S rRNA were measured in shNT and shATF4.HT1080 cells grown in suspension for 48 hours by RT-PCR. Data are represented as mean fold change compared with attached cultures for 3 independent experiments (n = 3, mean ± SD). $^{**}P < 0.01$, Student's t test.

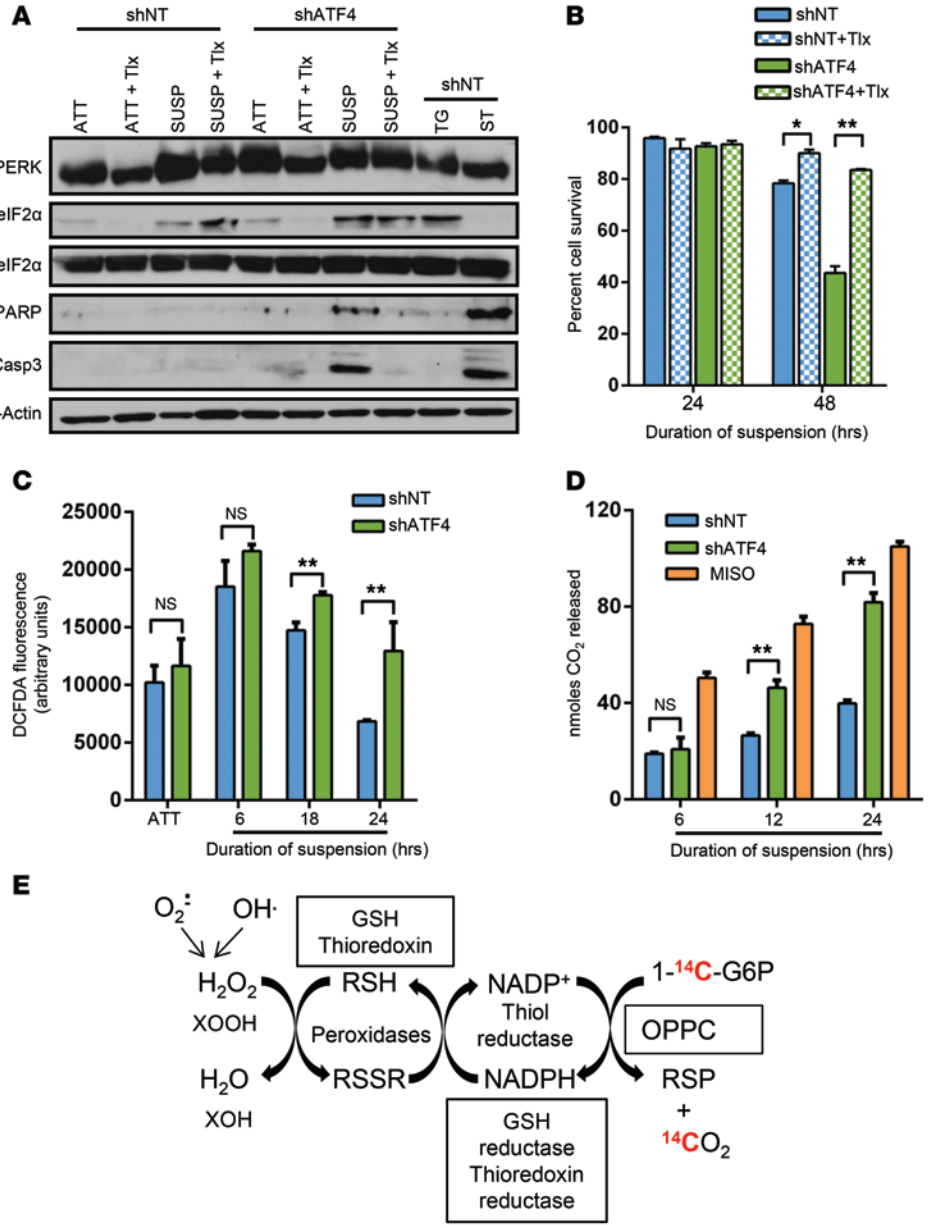

Figure 4. Absence of ATF4 induces oxidative stress following matrix detachment. (**A**) shNT and shATF4. HT1080 cells were treated with 50 μM Trolox (Tlx) in attached or suspension cultures for 48 hours. Immunoblots of indicated proteins as representative of 2 independent experiments are shown. (**B**) Mean cell survival of 3 independent experiments was measured in Trolox-treated cultures by Trypan blue exclusion and represented as mean ± SD (n = 3). *P < 0.05; **P < 0.01, Student's t test. (**C**) DCF-DA fluorescence levels were measured in shNT and shATF4. HT1080 cells at indicated time points. (**D**) Measurement of nanomoles of $^{14}CO_2$ (highlighted red in **E**) released at various time points from shNT and shATF4.HT1080 cells kept in suspension cultures or treated with 5 mM misonidazole (Miso) as positive control. Data for **C** and **D** are represented as the mean of 3 independent experiments (n = 3, mean ± SD). *P < 0.05; **P < 0.01, Student's t test. (**E**) Schematic representation of the OPPC and measured $^{14}CO_2$ (red).

of ATP production in the cells — both of which have been shown to induce ISR (37). Thus, the presence of the sustained ISR signaling is likely a reflection of the multiple types of stress conditions a cancer cell has to withstand when it loses cell-to-cell or matrix contact.

To measure the impact of ATF4 expression on levels of oxidative stress, we assayed 2′,7′-dichlorofluorescin diacetate (DCF-DA) fluorescence in shNT and shATF4.HT1080 cells grown in suspension for various time points. Compared with attached cultures, both shNT and shATF4.HT1080 cells showed significant upregulation of DCF-DA fluorescence levels at as early as 6 hours of suspension (Figure 4C). By 24 hours, shNT.HT1080 cells showed reduced DCF-DA fluorescence levels compared with shATF4 cells (Figure 4C). Persistently high fluorescence activity over time in shATF4.HT1080 cells suggests continuous accumulation of ROS in the absence of ATF4 followed by loss of matrix attachment.

As a secondary assay for levels of cellular oxidative stress, we used the oxidative pentose phosphate cycle (OPPC) assay. The OPPC is elevated following increased oxidative stress to maintain cellular redox status of the cells by maintaining the NADPH/$NADP^+$ ratio (39). Increased flux through OPPC can be detected by incubating cells in media supplemented with labeled D-[1-^{14}C] glucose and measuring released $^{14}CO_2$ over time (Figure 4D). A gradual accumulation of $^{14}CO_2$ was observed in both shNT.HT1080 and shATF4.HT1080 cells (Figure 4D). However, by 24 hours, there was significantly higher accumulation of $^{14}CO_2$ in shATF4.HT1080 cells compared with shNT cells, which was comparable to that induced by 5 mM misonidazole treatment (a potent prooxidant agent), suggesting increased metabolic flux through the OPPC (Figure 4E). Collectively, these results support a model in which absence of ATF4 results in progressively increased levels of oxidative stress that ultimately lead to sensitivity to anoikis.

ATF4 is a potent inducer of expression of the antioxidant gene HO-1 in response to anoikis. ATF4 transcriptionally regulates several antioxidant genes in response to oxidative stress, including *HO-1*, glutathione peroxidase 1 (*GPX1*), and superoxide dismutase 2 (*SOD2*) (40, 41). While *GPX1* and *SOD2* levels remained largely unchanged, *HO1* transcript levels were increased nearly 5-fold after 24 hours of suspension, in an ATF4-dependent manner (Figure 5A). Correlating with its transcript expression, the protein levels of HO-1 were significantly upregulated in both HT1080 and DLD1 cells placed in suspension for 24 hours (Figure 5B and Supplemental Figure 6A). Importantly, HO-1 protein levels were

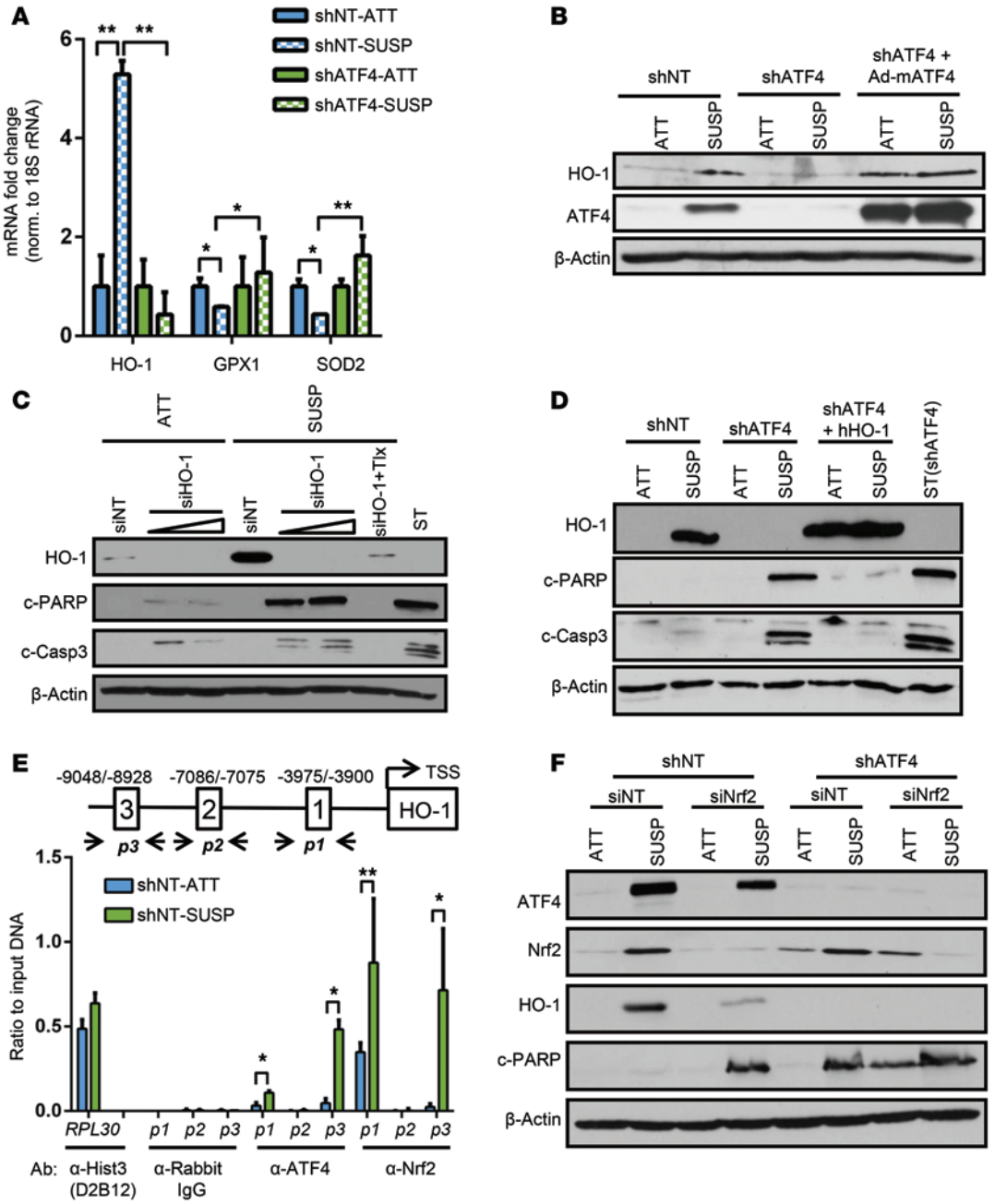

Figure 5. ATF4 induces expression of HO-1 in response to detachment-activated oxidative stress. (**A**) RT-PCR analysis of *HO1*, *GPX1*, and *SOD2* in shNT and shATF4.HT1080 cells grown in suspension for 48 hours. Data are represented as mean fold change compared with attached cultures for 3 independent experiments ($n = 3$, mean ± SD). $^*P < 0.05$; $^{**}P < 0.01$, Student's *t* test. (**B**) Expression of HO-1 in shNT and shATF4.HT1080 cells and adeno-mATF4–infected shATF4.HT1080 cells as measured by immunoblot analysis. (**C**) HT1080 cells were transfected with increasing amounts of siRNA against HO-1 (siHO-1) or siNT. Immunoblots for indicated proteins were measured. (**D**) shATF4.HT1080 cells with lentiviral-mediated overexpression of hHO-1 (shATF4 + hHO-1) were grown. Immunoblots for apoptosis markers were performed. (**E**) Schematic representation of AREs in the *HO1* promoter and primer sets (*p1*, *p2*, *p3*) indicating amplified regions encompassing the 3 ARE sites along with transcription start site (TSS). ChIP analysis was performed by either α-ATF4 or α-NRF2 antibody and by measuring enrichment at 3 AREs in human *HO1* promoter by RT-PCR. Antibodies against histone 3 (α-histone 3 D2B12) and rabbit IgG (α-rabbit IgG) were used as positive and negative controls, respectively, to amplify human RPL30 exon 3 of the human genome. Data are represented as ratio of input DNA (1:25) and presented as mean of 2 independent experiments ($n = 2$, mean ± SD). $^*P < 0.05$; $^{**}P < 0.01$, Student's *t* test. (**F**) Immunoblot analysis for indicated proteins in shNT and shATF4.HT1080 cells transfected with siNT or siNRF2 after 48 hours of suspension. All immunoblots are representative of 2 independent experiments.

undetectable in shATF4 cells and could be recovered by reexpression of mATF4 in both attached and suspension cultures (Figure 5B). Knockdown of HO-1 expression in HT1080 (Figure 5C) or DLD-1 cells (Supplemental Figure 6, B and C) resulted in a time-dependent increase in the levels of c-PARP and c–caspase 3, indicating that HO-1 expression is critical for cells to resist anoikis. DCF-DA fluorescence measurement in siNT and siHO-1 HT1080 showed significant ROS accumulation in the absence of HO-1 by

18 hours (Supplemental Figure 7A). Similarly, measurement of metabolic flux through OPPC showed higher $^{14}CO_2$ accumulation in siHO1 HT1080 cells as compared with the nontargeting control (Supplemental Figure 7B), confirming its antioxidant property to cope with increasing ROS production.

To further investigate the role of HO-1, shATF4.HT1080 cells were transfected with a lentiviral vector expressing full-length human HO-1 protein (hHO-1). Immunoblots confirmed elevated HO-1 protein levels compared with shATF4.HT1080 cells following 48 hours of suspension culture (Figure 5D). Critically, reexpression of HO-1 protein in shATF4.HT1080 blocked apoptosis (Figure 5D). Collectively, these results strongly suggest that induction of ATF4 following matrix detachment results in upregulation of HO-1 to cope with increased oxidative stress. Failure to induce such ATF4-mediated antioxidant response results in increased sensitivity to anoikis-mediated cell death.

ATF4 binds to HO1 promoter following anoikis. ATF4 regulates gene expression by directly binding to the C/EBP-ATF regulatory elements (CARE) in the promoters of its target genes (42). Analysis of *HO1* promoter did not reveal any canonical or putative ATF4-binding sites. However, *HO1* is a known direct target of NRF2, a master regulator of the antioxidant stress response (23). Previous reports had shown that antioxidant response elements (AREs) are present within the *HO1* promoter, and at least one study reported that ATF4 and NRF2 interact in vitro, suggesting potential coordinated function (40). We focused on 3 AREs in the *HO1* promoter, as they have been shown to be NRF2-binding sites. The AREs were amplified by the primer pairs *p1*, *p2*, and *p3* (Figure 5E). Of the 3 AREs, significant enhancement of ATF4 binding was observed by ChiP in ARE1 (–3975/–3900) and ARE3 (–9048/–8928) only in suspension cultures (Figure 5E and Supplemental Figure 7B). As a control, the histone H3 Lys 4–specific antibody used to amplify RPL30 exon 3 regions showed binding independent of stress conditions (Figure 5E). These data strongly suggest that ATF4 binds to 2 unique ARE sites in the *HO1* promoter, likely via an interaction with NRF2 to transcriptionally upregulate its expression following matrix detachment.

ATF4 and NRF2 coordinate to increase HO-1 expression during matrix detachment. During activation of the ISR following oxidative stress, PERK directly phosphorylates NRF2 to transcriptionally activate an antioxidant gene program (25). Following loss of matrix attachment, HT1080 cells exhibited increased NRF2 expression, which was sustained even after 48 hours of suspension (Figure 5F). Such induction of NRF2 could be critical, since NRF2 is widely regarded as the primary transcriptional inducer of HO-1 (23). Indeed, knockdown of NRF2 expression by siRNA (siNRF2) in shNT.HT1080 cells significantly decreased HO-1 expression following suspension compared with nontargeting control siRNA (Figure 5F). Expression of HO-1 was totally blocked when NRF2 expression was knocked down in shATF4.HT1080 cells (Figure 5F). Importantly, knockdown of NRF2 increased apoptosis in shNT and shATF4.HT1080 cells under suspension and copied the apoptotic phenotype of shATF4.HT1080 cells (Figure 5F). Furthermore we observed significant enrichment of NRF2 binding at ARE1 and ARE3 sites of the *HO1* promoter, which further increased in suspension conditions (Figure 5E).

Next, we wanted to determine whether binding of NRF2 to the *HO1* promoter is dependent on ATF4. Knocking down NRF2 in HT1080 cells (siNRF2) resulted in a significant reduction of binding of ATF4 in ARE1 and ARE3, suggesting that NRF2 is required for binding of ATF4 to the *HO1* promoter (Supplemental Figure 7C). However, ChIP analysis in shATF4.HT1080 cells showed no significant change in NRF2 binding to AREs in the *HO1* promoter (Supplemental Figure 7D). Together, these data strongly point toward a cooperative activity of ATF4 and NRF2 that increases *HO1* mRNA and protein levels and also show that absence of either one of these transcription factors compromises HO-1 induction under ECM detachment.

ATF4 is required for lung colonization by human fibrosarcoma cells. To test the consequences of ATF4 loss and inability to mount an effective anoikis in an in vivo system, we employed a lung colonization assay using luciferase-expressing shNT.HT1080 or shATF4.HT1080 cells (Supplemental Figure 6A). Colonization in this assay is dependent on the survival of the injected cells while in circulation as well as attachment of the cells. Luciferase activity of each cell line in vitro was comparable (data not shown). Both shNT and shATF4.HT1080 cell–injected mice showed robust luciferase activity in the chest cavity due to the apparent trapping of the cells in the lung capillaries. Because imaging of the mice was performed 4 hours after inoculation, these results indicate that the cells were viable at the time of injection. (Supplemental Figure 8A). The bioluminescent signal continued to increase in the mice with shNT.HT1080 cells with each weekly measurement, while no signal was detected in mice injected with either one of two distinct shATF4 clones (Supplemental Figure 8B). Of 7 mice injected with shNT.HT1080 cells, 6 developed sizeable lung colonies with increased H&E staining, while none of the mice injected with the shATF4 clones did (Supplemental Figure 8, C and D). The overall survival curves reflected this dramatic difference in lung colonization, as all of the mice with shNT.HT1080 lung colonies had to be euthanized due to tumor-related weight loss (Figure 6A). In contrast, all of the 11 shATF4.HT1080-injected mice survived, some more than 100 days after the intravenous injection (Figure 6A).

To further test whether ATF4 was required for effective lung colonization, shNT, shATF4, and adeno-mATF4.HT1080 cells were introduced into the nude mice via tail-vein injection (Figure 6B). Similar to the previous experiment, mice injected with the shNT.HT1080 cells had a marked increase in luciferase activity compared with those injected with shATF4.HT1080 cells. By 8 weeks after injection, the shNT.HT1080- and mATF4-reconstituted HT1080 cells showed comparable signals (Figure 6C). These data suggest that ATF4 not only rescues the cell's ability to form lung colonies, but also promotes survival during the initial stages when the cells cannot proliferate due to absence of matrix attachment. Moreover, expressing HO-1 in *trans* in ATF4-deficient cells resulted in a partial, but significant increase in luciferase activity as compared with shATF4.HT1080 cells (Figure 6D). Such partial recovery could be attributed to several other genes that are upregulated in response to tumor microenvironments in an ATF4-dependent manner. Overexpressing HO-1 also resulted in increased secondary metastatic sites (such as hind leg muscle and abdomen) and a decreased overall survival rate in mice compared with the shATF4 counterpart

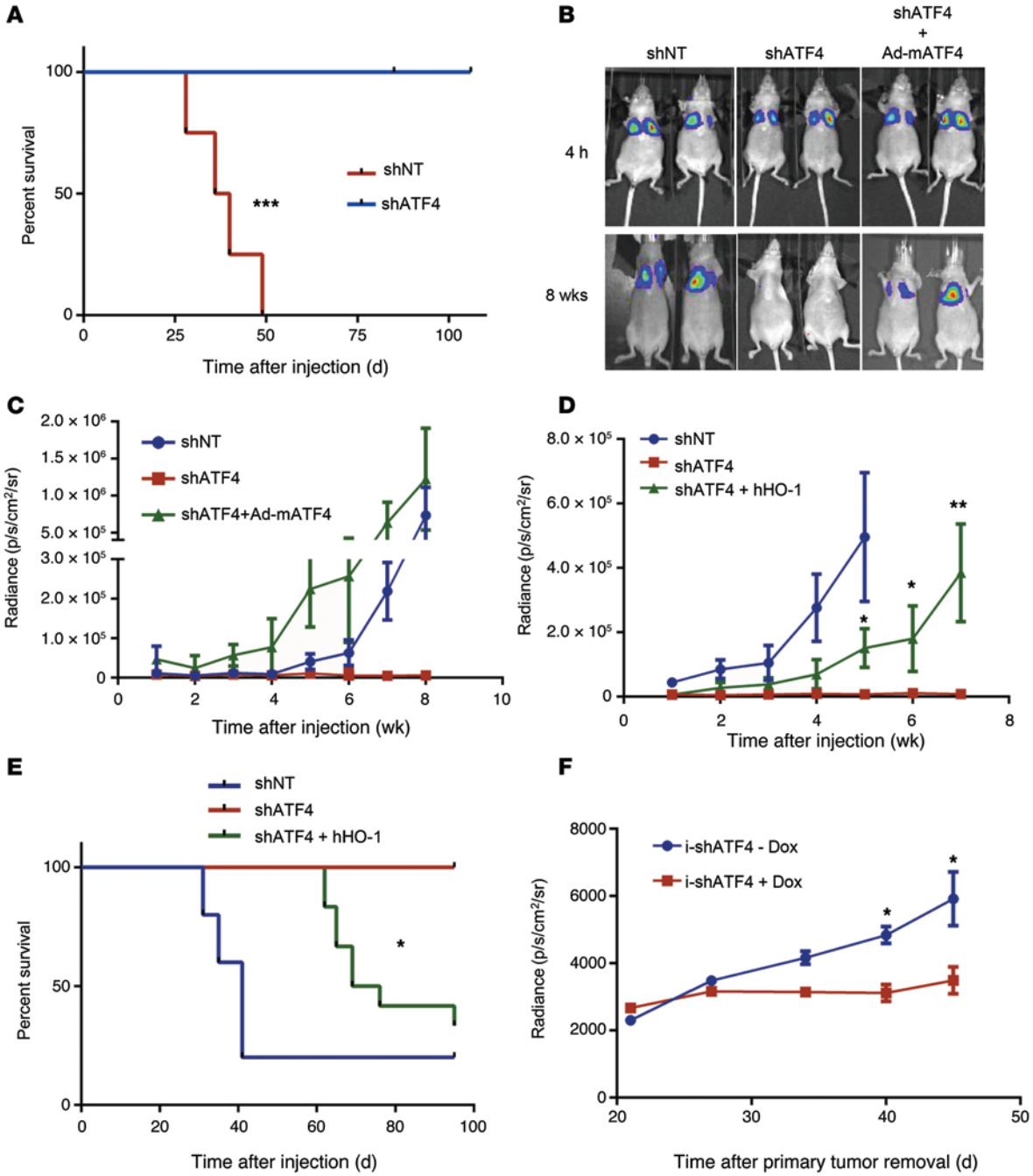

Figure 6. ATF4 and HO-1 promote fibrosarcoma lung colonization. (**A**) Kaplan-Meier survival analysis for mice injected by tail vein with shNT (n = 4) or shATF4 HT1080 clones (n = 8). ***P = 0.0002, log-rank test. (**B**) shNT (n = 5), shATF4 (n = 5), and ATF4 overexpressing (shATF4 + Ad-mATF4) HT1080 cells (n = 8) were injected intravenously, and bioluminescent images were obtained. Representative images from 4 hours after injection and 8 weeks after injection are shown. (**C**) Mean radiance (photon/s/cm^2/sr) from the chest/lung area of mice is plotted against time after injection (mean ± SEM). (**D**) shNT.HT1080 cells along with shATF4.HT1080 cells and HO-1–overexpressing cells (shATF4 + hHO-1) were injected. Mean radiance is plotted as a function of time (mean ± SEM). *P < 0.05; **P < 0.01, Student's t test. (**E**) Kaplan-Meier survival analysis for mice injected with shNT.HT1080 (n = 5), shATF4.HT1080 (n = 5), and shATF4+hHO-1.HT1080 (n = 10) cells (*P = 0.0285, log-rank test between groups of mice injected with shATF4.HT1080 and shATF4+hHO-1.HT1080 cells). (**F**) i-shATF4.HT1080 cells were injected on the right flank in female nude mice, and mice were administered water with or without 1 mg/ml Dox (+Dox, n = 8; –Dox, n = 7). Primary tumors were excised surgically when tumors reached approximately 400 mm^3, and bioluminescence from the chest/lung area was measured and plotted over time (days). Data are represented as mean ± SEM. *P < 0.05, Student's t test.

(Supplemental Figure 9, A–C, and Figure 6E). Serial lung sections from mice injected with shNT.HT1080 cells displayed high expression of ATF4 and HO-1 (Figure 7C) as well as moderate expression of LC3. Importantly, the highest levels of expression of these proteins showed extensive areas of colocalization in these tumors (arrows in Figure 7C), suggesting that ATF4 and HO-1 expression must play an important role in formation of lung colonies by HT1080 fibrosarcoma cells.

Finally, we utilized a flank xenograft tumor model to explore whether inducible loss of ATF4 plays a role in tumor metastasis. HT1080.i-shATF4 cl.4 cells were injected subcutaneously into the flanks of nude mice. After 2 days, mice were divided into 2 groups, and half were given Dox dissolved in their drinking water (+Dox). Primary tumors were removed when they reached approximately 400 mm^3 to allow for metastatic spread to form in the lungs. Compared with the –Dox (normal ATF4 levels) group, there was a decrease in the primary tumor volume in the +Dox (lower ATF4 levels) group (Supplemental Figure 10, A and B). More importantly, approximately 40 days following primary tumor removal, there was also a significant decrease in the metastatic tumor volume in the lungs in the mice treated with Dox (lower ATF4) (Figure 6F and Supplemental Figure 10C). Analysis of the lungs by H&E staining showed larger sized metastatic colonies in –Dox mice compared with the +Dox group (Supplemental Figure 10D).

HO-1 is expressed in metastatic human tumors. Interrogation of publicly available data sets from 1,406 lung cancer patients showed a significantly lower probability for overall survival rate in patients with higher HO-1 tumor expression levels (Figure 7A and ref. 43). Similarly, higher expression of *HO1* (transcript levels ≥ 2-fold) in glioblastoma patients also predicted a significantly reduced survival rate (Figure 7B).

Next, we analyzed the pattern of HO-1 expression in tumors isolated from cancer patients. Immunochemistry analysis with HO-1–specific antibody (Supplemental Figure 11A) determined that HO-1 was not highly expressed in histopathologically normal mesenchymal or epithelial tissue (Supplemental Table 2 and Supplemental Figure 11B). We also detected very low expression of HO-1 in primary breast and sarcoma tumors with no known lymphatic involvement or metastasis at the time of surgical resection (Supplemental Figure 12, A and B). ATF4 expression was quite variable in these tumors (Supplemental Figure 12, A and B). Similarly, absence of HO-1 was also observed in human leiomyosarcoma samples with no confirmed metastasis at the time of surgical resection (Supplemental Figure 12C). In contrast, high HO-1 expression was detected in samples from primary breast with positive lymph node infiltration and metastatic sarcoma (to the brain) (Figure 7, D and E). Importantly, there was extensive colocalization between high ATF4 and HO-1 expression in both these metastatic tumor lesions (Figure 7, D and E). The results above, coupled with the correlation of HO-1 levels with worse outcome in lung and glioma cancer patients, support the notion that high HO-1 expression in the primary tumor may confer on transformed cells the ability to resist conditions of matrix detachment and contribute to metastatic behavior.

Discussion

The metastatic process requires that transformed cells acquire several characteristics to overcome normal tissue homeostatic mechanisms. In epithelial cell tumors, EMT is critically important for migration and invasion into the ECM (44). However, in tumors of mesenchymal cell origin (such as sarcomas, which were investigated here), the role of EMT is less clear. Cell migration and invasion into the ECM are also key requirements for intravasation and subsequent colonization. Our in vitro results indicate that, for these 2 processes, ATF4 is dispensable, at least in the mesenchymal cell system we tested.

Loss of attachment to the proper ECM can lead to binding and proliferation of cells to an inappropriate substrate (45). To counterbalance this potentially detrimental effect, the process of anoikis has evolved to ensure proper development of multicellular organisms and also serve as an important barrier mechanism to prevent dysplastic growth (20). However, metastatic cancer cells can elicit elaborate mechanisms to escape anoikis while detaching from the ECM of their primary site. Most mechanisms elicited to prevent anoikis impinge on blocking the caspase-mediated apoptotic pathways by regulating antiapoptotic factors such as BCL2 as well as suppressing proapoptotic factors such as BID, BAX, and BIM. Such pathways are mediated by cell-surface effectors such as integrin-mediated activation of PI3K/AKT pathways as well as activation of receptor tyrosine kinases (46, 47). However, recent studies have demonstrated that integrin-independent signaling pathways such as the UPR can play a key role in regulating anoikis (22). Our results indicate that ATF4 (an effector of PERK) plays a critical role in executing the ISR response for survival of anoikis (Figure 8).

Our data suggest a dual mechanism of ATF4 to provide anoikis resistance. One mechanism involves activation of a cytoprotective autophagy program by regulating important autophagy-related genes such as *ATG5*, *ATG7*, and *ULK1*. Our data are in agreement with a recent study that demonstrated the role of PERK-mediated cytoprotective autophagy in suspended luminal breast cancer cells (MCF10A) in vitro and in vivo (22). Our results also suggest a complementary mechanism by which ATF4 confers anoikis resistance. It has been reported that ROS generated during matrix detachment is caused by the small GTPase RAC1 upon engagement with integrins and is beneficial for cancer cells, as it activates the PI3K/AKT pathway (48, 49). While increased ROS levels can have proliferative roles, unbalanced and unmitigated ROS increase can result in organelle destruction and, ultimately, cell death. We observed that chronic oxidative stress is induced following loss of matrix attachment in the absence of ATF4, which led to sensitization of cells to anoikis. Importantly, our results indicate that the potent antioxidant Trolox can rescue detached cells lacking ATF4, underscoring the fact that it is the antioxidant properties of ATF4 that are critical for anoikis resistance. Additionally, it has been shown by Schafer et al. that antioxidants can also prevent anoikis by increasing intracellular ATP levels — a mechanism involving enhancing fatty acid oxidation (37). This study also shows that the effect of matrix detachment on intracellular ATP levels can be phenocopied by overexpression of oncogenes such as ERBB2 (37). Interestingly, HT1080 cells have an activating N-RAS mutation and DLD1 cells have an activating K-RAS mutation. Mutations in RAS such as $HRAS^{V12}$ have been shown to activate UPR, and deactivation of important regulators of UPR such as IRE1, XBP1, ATF6, and ATF4 induces cellular apoptosis in the presence of the oncogene expression (50). Furthermore, Croft et al. have shown that hyperactive oncogenic signaling through RAS or $BRAF^{V600E}$ activates MEK/ERK signaling, which is required to adapt the cells to cope with increased levels of inherent endoplasmic stress (51).

The antioxidant properties of ATF4 have been well documented, as it transcriptionally induces several antioxidant genes

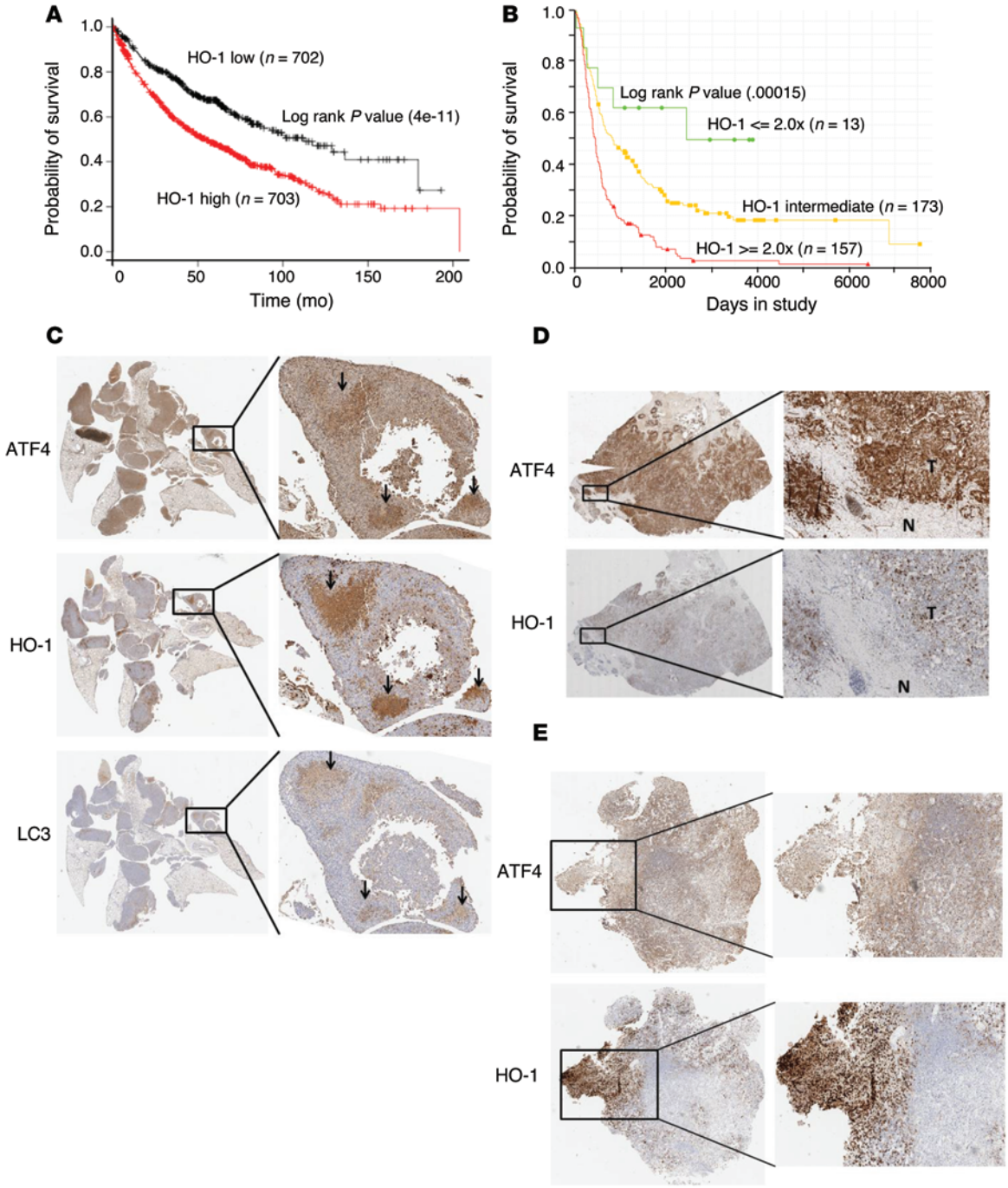

Figure 7. High HO-1 expression correlates with metastasis and reduced overall survival in patients. (**A**) Probability of overall survival in 1406 patients with lung cancer stratified on low (black) versus high (red) expression levels of HO-1 were obtained from Kaplan-Meier Plotter/lung cancer (http://www.kmplot.com/lung). (**B**) Probability of overall survival in glioblastoma patients with either upregulated (≥2-fold over the mean), downregulated (≤2-fold over the mean), or intermediate *HO1* expression is from the Georgetown Database of Cancer (G-DOC Plus) (https://gdoc.georgetown.edu/gdoc/), with *n* representing the patient number for each group. Statistical significance was calculated based on log-rank test. (**C**) Immunohistochemical analysis of serial lung sections from mice injected with shNT.HT1080 cells using antibodies against ATF4, HO-1, and LC3. Insets show areas of colocalization in the 3 detected proteins. **D** and **E** show expression of HO-1 and ATF4 from surgical specimens from primary breast tumor with known involvement of lymph node metastasis (**D**) and brain metastatic lesion from a patient with a primary sarcoma (**E**). T, tumor region; N, normal tissue. Original magnification, ×2, ×5 (insets) (**C**); ×2, ×4 (insets) (**D** and **E**).

following ER stress, which allows amelioration of ROS (2, 26, 38). We found that the mRNA and protein levels of HO-1 were substantially induced following matrix detachment. Intriguingly, HO-1 is also a target of HIF1α, and it is upregulated in renal cell carcinoma and prostate tumors and confers resistance to radiotherapy- and photodynamic therapy–induced cellular toxicity (52–54). The role of HO-1 toward tumor metastasis is largely unclear. Murine melanoma cells (B16F10, S91, and SK-mel188) overexpressing HO-1 have also been shown to increase metastatic lesions in lungs by augmenting vascularization and upregulation of VEGF expression (55). Similarly, transplantation of pancreatic tumors overexpressing HO-1 in rats results in a higher incidence of metastasis to lungs (56). One mechanism by which HO-1 potentiates tumor metastasis involves genes regulating ECM, such as the matrix metalloproteinases MMP9 and MMP2, which are upregulated (~5-fold) in lung metastatic tumors (57). Other reported mechanisms by which HO-1 is thought to regulate metastasis include upregulation of thymosin-β4 (T β4), which has been shown to be elevated in HO-1–overexpressing melanoma cells and has been shown to induce metastasis in melanoma, fibrosarcomas, and squamous cell carcinomas (55, 58, 59). A third proposed mechanism involves activation of HYAL1 (hyaluronidase), which has been also shown to be overexpressed in HO-1–elevated tumors and has been implicated as a biomarker for metastatic potential of the tumor (55, 60). Finally, HO-1 has been shown extensively as a proangiogenic factor, controlling important regulators, such as VEGF and basic FGF (bFGF) (61). These results support an emerging model in which HO-1 plays a central role in upregulating multiple prometastatic activities in multiple tumor systems, thereby making it an attractive target to prevent both primary and metastatic tumor growth.

Studies with HO-1 inhibitor zinc protoporphyrin IX (ZnPPIX), a heme analogue that inhibits HO-1 enzymatic activity, have shown promising results toward reducing primary tumor growth cell lymphoma, lung cancer, and sarcoma in mice (62). One of the major issues for ZnPPIX is its solubility, which makes it difficult for it to work in vivo. However, recent developments, such as highly water soluble PEG-ZnPPIX and SMA-ZnPPIX, have shown considerable improvement in its antitumor potential and tumor drug retention as well as reduced side effects in mice (63).

Even though the protumorigenic properties of HO-1 have been well documented, the precise mechanism by which HO-1 exerts its effects on autophagy is not well established. Under physiological conditions, increased HO-1 expression has been shown to induce autophagy to remove damaged mitochondria and repress oxidative stress that can lead to tumorigenesis (64, 65). However, once a malignancy has been established, increased levels of ROS have been shown to promote both primary and metastatic growth (66).

Both endoplasmic reticulum stress and oxidative stress have been shown to induce activation of the PERK-dependent arm of the UPR (4, 67). PERK has been shown to activate NRF2 independently of eIF2α-P–mediated ATF4 upregulation, and both NRF2 and ATF4 have demonstrated antioxidant properties. Collectively, our data provide what we believe is a new mechanistic insight into how PERK-mediated ATF4 and NRF2 pathways work in conjunction to activate an antioxidant response to cope with increasing ROS. Our results reveal that an important intersection node between PERK-eIF2α-ATF4 and PERK-NRF2 signaling toward conferring anoikis resistance is the transcriptional upregulation of *HO1*. NRF2 and ATF4 accumulate, interact, and bind to ARE sites in the *HO1* promoter; these are predominantly known to be binding sites for NRF2. This common signaling pathway originating from PERK further adds to the growing evidence that suggests that PERK could potentially be exploited as a therapeutic target (4, 7, 68) to induce anoikis in circulating tumor cells and prevent metastatic growth.

Methods

Chemicals

TG (catalog T9033), Trolox (catalog 238813), puromycin (catalog P9620), and Dox (catalog D9891) were purchased from Sigma-Aldrich. Spautin-1 was obtained from Millipore (catalog 567569, Calbiochem). Methylcellulose (catalog 64670) and poly-HEMA (catalog 772542) for suspension cultures were also obtained from Sigma-Aldrich. PERK inhibitor GSK414 was provided by Jonathan Axten (GlaxoSmithKline) (28).

Cell culture and generation of stable cell lines

HT1080 human fibrosarcoma cells and DLD1 human colorectal fibrosarcoma cells were obtained from ATCC (HT1080-CCL-121 and DLD1-CCL-221) and were cultured in DMEM supplemented with penicillin, streptomycin, and 10% FBS. Cells at a density of 5×10^5/ml were placed in suspension culture in media with 0.5 % methylcellulose to prevent clumping and were plated on tissue culture plates coated overnight with poly-HEMA (6 mg/ml in 95% ethanol) at 37°C for drying. Following suspension, the cells were centrifuged and washed twice with ice-cold PBS for protein measurement. HT1080 and DLD1 cells stably expressing shNT and shATF4.HT1080 and DLD1 cells as well as shGCN2.HT1080 cells were previously described (11). HT1080 cells stably transfected with shPERK (shPERK.HT1080) were provided by J. Alan Diehl (69). i-shNT and i-shATF4.HT1080 cells were created by stably transfecting HT1080 cells with TRIPZ shNT (i-shNT) or shATF4 (i-shATF4) vectors (Thermo Scientific) and selecting with 2 μg/ml puromycin to obtain stable clones. Dox (1 μg/ml) was used to induce the expression of the shRNA. The CAS9/CRISPR system targeted to exon 2 of the *ATF4*-coding sequence was used to generate pSp-CRISPR-ATF4 cells from HT1080 human fibrosarcoma cells. shATF4.HT1080, pSp-CRISPR-ATF4, and i-shATF4 were grown in media supplemented with nonessential amino acids and 55 μM β-mercaptoethanol. Rescue of ATF4 expression was performed by transducing shATF4.HT1080 or shPERK.HT1080 cells with adenovirus encoding full-length mATF4 (Ad-mATF4) as described previously (11). Overexpression of HO-1 was performed by lentiviral transfection of hHO-1-IRES-GFP (Precision LentiORFs, Thermo Scientific) to shATF4.HT1080 cells and selected for 15 μg/ml blasticidin. For bioluminescent imaging, cells were transfected with a constitutively expressed luciferase plasmid and then selected with 500 μg/ml G418. ON-TARGETplus siRNAs against human *ATG5* (catalog L-004374), *ATG7* (catalog L-020112), *ULK1* (catalog L-005049), *HO1* (catalog L-006372), and *NRF2* (catalog L-003755) were obtained from Thermo Scientific. Efficiency of knockdown was confirmed by immunoblot analysis.

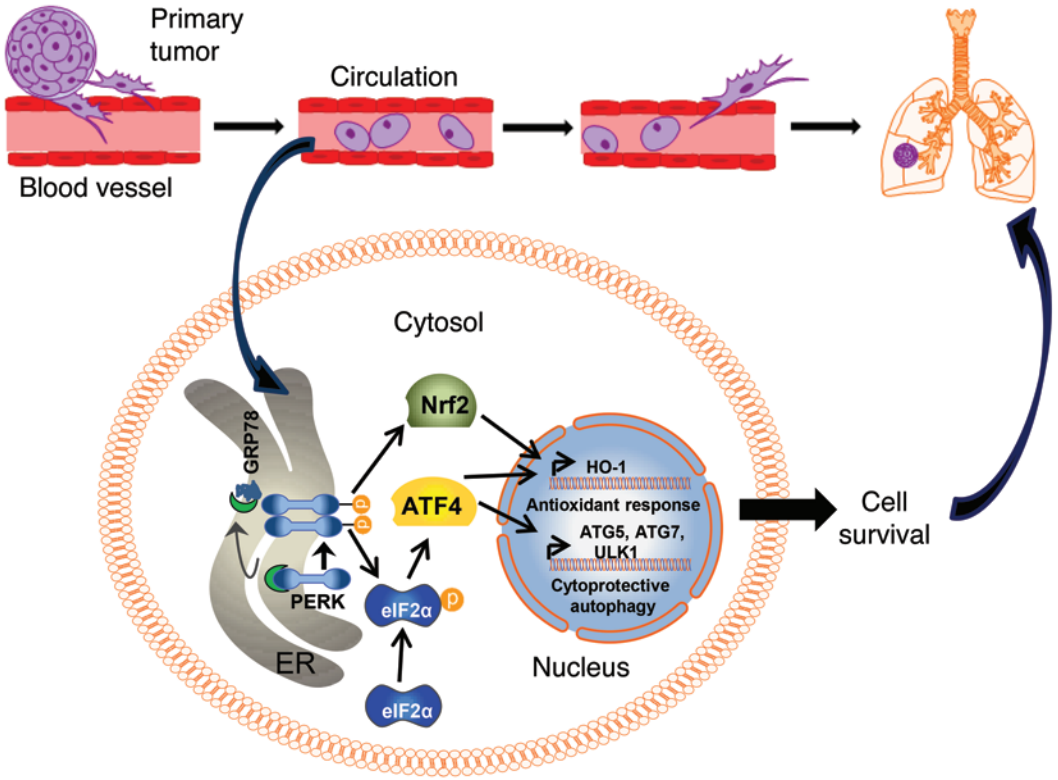

Figure 8. Model for involvement of HO-1 in ATF4-mediated metastasis. Detachment of tumor cells from ECM results in activation of the PERK pathway (and likely the IRE1 and ATF6 pathways), which are normally kept inactive by the endoplasmic reticulum–resident chaperone protein GRP78 (for clarity, only the PERK pathway, which is the focus of this work, is shown here). Activation of PERK mediates eIF2α phosphorylation and translational upregulation of ATF4. In turn, ATF4 activates a cytoprotective autophagy program by upregulating key autophagy genes. ATF4 also cooperates with NRF2 (directly activated by PERK) to activate the antioxidant protein HO-1 to counter increasing oxidative stress following loss of ECM. The combined action of the autophagic and antioxidant effector pathways of the PERK arm of the UPR enables tumor cells to survive longer in circulation and results in increased rates of formation of secondary metastatic sites.

Immunoblot analysis

Immunoblotting was performed as previously described (3). The primary antibody against ATF4 was purchased from Santa Cruz Biotechnology Inc.: anti–rabbit ATF4 (clone C-20, catalog sc-200). The following antibodies were purchased from Cell Signaling Technologies: anti-rabbit phospho-eIF2α (Serine 51) (catalog 9721), anti-rabbit eIF2α (catalog 9722), anti-rabbit CHOP (clone D46F1, catalog 5554), anti-rabbit human-specific c-PARP (Asp214) (catalog 9541), anti-rabbit cleaved caspase 3 (Asp175) (catalog 9661), anti-rabbit PERK (clone D11A8, catalog 5683), anti-rabbit LC3B (catalog 2775), anti-rabbit p62 (catalog 5114), anti-rabbit ATG5 (catalog 2630), anti-rabbit ATG7 (catalog 2631), anti-rabbit NRF2 (clone D1Z9C, catalog 12721), anti-rabbit XBP1s (clone D2C1F, catalog 12782), anti-rabbit Ku80 (catalog 2753), and anti-rabbit HO-1 (clone P240, catalog 5061). The following antibodies were purchased from Sigma-Aldrich: anti-rabbit ULK1 (catalog A7481) and anti-mouse β-actin (clone AC-40, catalog A3853). Anti-rabbit phospho-PERK (Threonine 982) was provided by Kirk Staschke (Eli Lilly). Anti-rabbit ATF6 antibody was provided by Ronald C. Wek (Indiana University School of Medicine, Indianapolis, Indiana, USA) (70).

Real-time quantitative PCR

RNA was isolated with TRIzol Reagent (Ambion). Reverse transcription was performed using AMV Reverse Transcriptase (Promega). Real-time quantitative PCR was done using Power SYBR Green PCR Master Mix (Applied Biosystems) and was analyzed with the Applied Biosystems 7300 Real-Time PCR System. PCR primers (Invitrogen) used are mentioned in Supplemental Table 1. Relative mRNA levels were quantified using the standard curve method. Experiments were done in triplicate and are represented as mean plus SD.

Cell viability

Cell viability was also measured by 0.1% Trypan blue and was digitally analyzed and counted by Nexcelom Cellometer Auto X4 Cell Counter (Nexcelom Bioscience). All viability experiments were repeated as 3 independent experiments, and mean percentage of cell survival was calculated along with SD. Student's *t* test was used for calculating statistical significance.

ROS measurements

shNT and shATF4.HT1080 as well as siNT and siHO-1.HT1080 cells were grown in attached or suspension conditions for indicated periods of time. Cells were trypsinized, resuspended in PBS containing 10 μM DCF-DA (Sigma-Aldrich), and incubated at 37°C for 30 minutes. Levels of fluorescence were measured by Fluoroskan Ascent (Thermo Electron Corporation). Results are representative of 3 independent experiments ± SD, and statistical significance was obtained by Student's *t* test.

$^{14}CO_2$ release assay

Of corresponding cells, 2.5×10^5 cells were plated in 25-mm glass scintillation vials coated with Poly-HEMA (suspension culture). Cells were incubated in DMEM without glucose but supplemented with 5 mM D-[1-^{14}C] glucose (PerkinElmer) and 5 mM sodium bicarbonate. Vials were sealed with a stopper to prevent leakage of CO_2. OPPC was determined by measuring released $^{14}CO_2$ trapped on a Whatman GF/B glass fiber filter that was saturated with 0.1 ml of 5% KOH. Injecting 6N acetic acid into the vials stopped reactions, and the radioactivity from the filter was measured by PerkinElmer Tri-Carb 2810 TR scintillation counter. Data were normalized and represented relative to radioactive media with no cells as mean of 3 independent experiments.

ChIP

ChIP assays were performed on 1×10^7 shNT.HT1080 and shATF4.HT1080 as well as siNT- and siNRF2-transfected cells using the Simple ChIP Enzymatic Chromatin IP Assay Kit (Cell Signaling, catalog 9003) per the manufacturer's protocol. Immunoprecipitation reactions employed antibodies against anti-rabbit ATF4 (clone C-20, catalog sc-200, Santa Cruz Biotechnology Inc.), anti-rabbit NRF2 (catalog 12721, Cell Signaling Technology), anti-rabbit histone H3 (clone D2B12, catalog 4620, Cell signaling Technologies), and normal rabbit IgG (catalog 27129, Cell Signaling Technologies). Real-time quantitative PCR was used to analyze immunoprecipitated DNA fragments. DNA were designated as *p1*, *p2*, and *p3*; primer sets are provided in Supplemental Table 1. Primers for RPL30 were provided with the abovementioned kit. Values are the mean of 2 independent experiments with SD as indicated. Statistical analysis was done by 2-tailed Student's *t* test.

Animals

Female athymic nude mice (Nu/Nu) from Charles River Laboratories were used for all in vivo experiments. Animals were housed at the University of Pennsylvania animal facility. 5×10^5 shNT.HT1080 and shATF4.HT1080 as well as shATF4.HT1080 cells infected with adeno-mATF4 or Lenti-IRES-hHO-1 plasmid were suspended in a total volume of 100 μl PBS and injected into the tail veins. Mice were imaged weekly for lung colony formation. Animals were euthanized when they had lost 15% or more of their body weight.

Primary tumor removal and metastasis

Female athymic nude mice (Nu/Nu) were injected in the flank with 2×10^6 i-shATF4.HT1080 cells. Two days following injections, mice were administered drinking water containing Dox (1 mg/ml) and sucrose (25 g/liter). Control mice were placed on sucrose water alone. Tumors were excised when they reached about 400 mm^3. Weights of the mice were observed after surgery, and mice were euthanized when they had lost more than 15% of their body weight. Metastatic tumor growth was monitored by bioluminescence imaging.

Bioluminescent imaging

Prior to imaging, mice were anesthetized, injected with 200 μl of 50 μg/ml D-luciferin (Regis Technologies), and imaged using the Carestream Imager (Carestream Health Inc.) or the IVIS Spectrum (PerkinElmer). The average relative light intensity of the chest/lung area was measured utilizing either Carestream Molecular Imaging software (Carestream Health Inc.) or Living Image software (PerkinElmer). Lungs were harvested in 10% formalin; this was followed by tissue fixation and paraffin embedding.

Immunohistochemistry

Frozen human tissue samples were obtained from the Abramson Cancer Center Tumor Tissue Bank (University of Pennsylvania). Paraffin-embedded tissue slides from human as well as mouse lungs were deparaffinized and rehydrated, and antigen retrieval was performed using 10 mM sodium citrate (pH 6.0). Inactivation of endogenous peroxidase was performed with 3% hydrogen peroxide, followed by blocking with 5% normal goat serum. Immunohistochemistry on serial tissue sections was performed with monoclonal anti-mouse HO-1 primary antibody (1:100, catalog NBP1-97507, Novus Biologicals), monoclonal anti-mouse ATF4 (1:250, clone 3E4C5, catalog 60035-1-Ig, Proteintech), and monoclonal anti-mouse LC3B (1:100, clone 5F10, catalog 0231-100, Nanotools Antibodies). Images were scanned and analyzed by Aperio Imagescope (Leica Biosystems).

For additional information, see Supplemental Methods.

Statistics

All graphs were generated and all statistics (Student's *t* test and log-rank test) were performed with GraphPad Prism software (GraphPad Software Inc.). Statistical analysis was performed with Student's 2-tailed *t* test. *P* values of less than 0.05 were considered significant.

Study approval

Animals. All animal experiments were approved by the University of Pennsylvania IACUC and were performed in accordance with NIH and University of Pennsylvania guidelines.

Human tumor samples. All human tissue samples were obtained from the Tumor Tissue/Biospecimen Bank core facility at the University of Pennsylvania School of Medicine. Informed consent was obtained under a protocol reviewed and approved of by the Institutional Review Board at the University of Pennsylvania (IRB protocol 807537).

Acknowledgments

We thank Julie Czupryna (Small Animal Imaging Facility, University of Pennsylvania) for providing technical guidance for imaging studies, Amy F. Ziober (Pathology Clinical Service Center, University of Pennsylvania) for tissue immunohistochemistry, and Mauricio Reginato (Drexel University, Philadelphia, Pennsylvania, USA) for providing protocols for suspension cultures. We thank Kirk Staschke (Eli Lilly) for providing phospho-specific PERK antibody. We also thank Vladimir M. Popov and Shannon Gallagher Colombo (University of Pennsylvania) for critical reading of the manuscript. This work is supported by NIH grants R01CA094214 and NIH P01CA165997 (to C. Koumenis). I.I. Verginadis is supported by a postdoctoral fellowship from the Bodossaki Foundation (Greece).

Address correspondence to: Constantinos Koumenis, Department of Radiation Oncology, Perelman School of Medicine, University of Pennsylvania, Smilow Centre for Translational Research, Room 8-124, 3400 Civic Center Blvd., Bldg 421, Philadelphia, Pennsylvania 19104-5156, USA. Phone: 215.898.0076; E-mail: costas.koumenis@uphs.upenn.edu.

Carly M. Sayers's present address is: Johnson and Johnson, Skillman, New Jersey, USA.

1. Finger EC, Giaccia AJ. Hypoxia, inflammation, and the tumor microenvironment in metastatic disease. *Cancer Metastasis Rev*. 2010;29(2):285–293.
2. Harding HP, et al. An integrated stress response regulates amino acid metabolism and resistance to oxidative stress. *Mol Cell*. 2003;11(3):619–633.
3. Koumenis C, et al. Regulation of protein synthesis by hypoxia via activation of the endoplasmic reticulum kinase PERK and phosphorylation of the translation initiation factor eIF2alpha. *Mol Cell Biol*. 2002;22(21):7405–7416.
4. Walter P, Ron D. The unfolded protein response: from stress pathway to homeostatic regulation. *Science*. 2011;334(6059):1081–1086.
5. Harding HP, et al. Regulated translation initiation controls stress-induced gene expression in mammalian cells. *Mol Cell*. 2000;6(5):1099–1108.
6. Vattem KM, Wek RC. Reinitiation involving upstream ORFs regulates ATF4 mRNA translation in mammalian cells. *Proc Natl Acad Sci U S A*. 2004;101(31):11269–11274.
7. Diehl JA, Fuchs SY, Koumenis C. The cell biology of the unfolded protein response. *Gastroenterology*. 2011;141(1):38–41.
8. Fels DR, Koumenis C. The PERK/eIF2alpha/ATF4 module of the UPR in hypoxia resistance and tumor growth. *Cancer Biol Ther*. 2006;5(7):723–728.
9. Blais JD, et al. Activating transcription factor 4 is translationally regulated by hypoxic stress. *Mol Cell Biol*. 2004;24(17):7469–7482.
10. Bi M, et al. ER stress-regulated translation increases tolerance to extreme hypoxia and promotes tumor growth. *EMBO J*. 2005;24(19):3470–3481.
11. Ye J, et al. The GCN2-ATF4 pathway is critical for tumour cell survival and proliferation in response to nutrient deprivation. *EMBO J*. 2010;29(12):2082–2096.
12. Bobrovnikova-Marjon E, et al. PERK promotes cancer cell proliferation and tumor growth by limiting oxidative DNA damage. *Oncogene*. 2010;29(27):3881–3895.
13. Igarashi T, et al. Clock and ATF4 transcription system regulates drug resistance in human cancer cell lines. *Oncogene*. 2007;26(33):4749–4760.
14. Tanabe M, et al. Activating transcription factor 4 increases the cisplatin resistance of human cancer cell lines. *Cancer Res*. 2003;63(24):8592–8595.
15. Ameri K, Lewis CE, Raida M, Sowter H, Hai T, Harris AL. Anoxic induction of ATF-4 through HIF-1–independent pathways of protein stabilization in human cancer cells. *Blood*. 2004;103(5):1876–1882.
16. Nagelkerke A, et al. Hypoxia stimulates migration of breast cancer cells via the PERK/ATF4/LAMP3-arm of the unfolded protein response. *Breast Cancer Res*. 2013;15(1):R2.
17. Suzuki T, Osumi N, Wakamatsu Y. Stabilization of ATF4 protein is required for the regulation of epithelial-mesenchymal transition of the avian neural crest. *Dev Biol*. 2010;344(2):658–668.
18. Yilmaz M, Christofori G. EMT, the cytoskeleton, and cancer cell invasion. *Cancer Metastasis Rev*. 2009;28(1–2):15–33.
19. Bonnomet A, et al. Epithelial-to-mesenchymal transitions and circulating tumor cells. *J Mammary Gland Biol Neoplasia*. 2010;15(2):261–273.
20. Taddei ML, Giannoni E, Fiaschi T, Chiarugi P. Anoikis: an emerging hallmark in health and diseases. *J Pathol*. 2012;226(2):380–393.
21. Simpson CD, Anyiwe K, Schimmer AD. Anoikis resistance and tumor metastasis. *Cancer Lett*. 2008;272(2):177–185.
22. Avivar-Valderas A, et al. PERK integrates autophagy and oxidative stress responses to promote survival during extracellular matrix detachment. *Mol Cell Biol*. 2011;31(17):3616–3629.
23. Gozzelino R, Jeney V, Soares MP. Mechanisms of cell protection by heme oxygenase-1. *Annu Rev Pharmacol Toxicol*. 2010;50:323–354.
24. Li N, et al. Nrf2 is a key transcription factor that regulates antioxidant defense in macrophages and epithelial cells: protecting against the proinflammatory and oxidizing effects of diesel exhaust chemicals. *J Immunol*. 2004;173(5):3467–3481.
25. Cullinan SB, Zhang D, Hannink M, Arvisais E, Kaufman RJ, Diehl JA. Nrf2 is a direct PERK substrate and effector of PERK-dependent cell survival. *Mol Cell Biol*. 2003;23(20):7198–7209.
26. Cullinan SB, Diehl JA. Coordination of ER and oxidative stress signaling: the PERK/Nrf2 signaling pathway. *Int J Biochem Cell Biol*. 2006;38(3):317–332.
27. Hetz C, Chevet E, Harding HP. Targeting the unfolded protein response in disease. *Nat Rev Drug Discov*. 2013;12(9):703–719.
28. Axten JM, et al. Discovery of 7-methyl-5-(1-{[3-(trifluoromethyl)phenyl]acetyl}-2,3-dihydro-1H-indol-5-yl)-7H-p yrrolo[2,3-d]pyrimidin-4-amine (GSK2606414), a potent and selective first-in-class inhibitor of protein kinase R (PKR)-like endoplasmic reticulum kinase (PERK). *J Med Chem*. 2012;55(16):7193–7207.
29. Bhattacharya S, et al. Anti-tumorigenic effects of Type 1 interferon are subdued by integrated stress responses. *Oncogene*. 2013;32(36):4214–4221.
30. Cullinan SB, Zhang D, Hannink M, Arvisais E, Kaufman RJ, Diehl JA. Nrf2 is a direct PERK substrate and effector of PERK-dependent cell survival. *Mol Cell Biol*. 2003;23(20):7198–7209.
31. Hippert MM, O'Toole PS, Thorburn A. Autophagy in cancer: good, bad, or both? *Cancer Res*. 2006;66(19):9349–9351.
32. White E. Deconvoluting the context-dependent role for autophagy in cancer. *Nat Rev Cancer*. 2012;12(6):401–410.
33. Liu J, et al. Beclin1 controls the levels of p53 by regulating the deubiquitination activity of USP10 and USP13. *Cell*. 2011;147(1):223–234.
34. Rouschop KM, et al. The unfolded protein response protects human tumor cells during hypoxia through regulation of the autophagy genes MAP1LC3B and ATG5. *J Clin Invest*. 2010;120(1):127–141.
35. Pike LR, et al. Transcriptional up-regulation of ULK1 by ATF4 contributes to cancer cell survival. *Biochem J*. 2013;449(2):389–400.
36. Rzymski T, et al. Regulation of autophagy by ATF4 in response to severe hypoxia. *Oncogene*. 2010;29(31):4424–4435.
37. Schafer ZT, et al. Antioxidant and oncogene rescue of metabolic defects caused by loss of matrix attachment. *Nature*. 2009;461(7260):109–113.
38. Lange PS, et al. ATF4 is an oxidative stress-inducible, prodeath transcription factor in neurons in vitro and in vivo. *J Exp Med*. 2008;205(5):1227–1242.
39. Tuttle SW, et al. Detection of reactive oxygen species via endogenous oxidative pentose phosphate cycle activity in response to oxygen concentration: implications for the mechanism of HIF-1alpha stabilization under moderate hypoxia. *J Biol Chem*. 2007;282(51):36790–36796.
40. He CH, et al. Identification of activating transcription factor 4 (ATF4) as an Nrf2-interacting protein. Implication for heme oxygenase-1 gene regulation. *J Biol Chem*. 2001;276(24):20858–20865.
41. Han J, et al. ER-stress-induced transcriptional regulation increases protein synthesis leading to cell death. *Nat Cell Biol*. 2013;15(5):481–490.
42. Kilberg MS, Shan J, Su N. ATF4-dependent transcription mediates signaling of amino acid limitation. *Trends Endocrinol Metab*. 2009;20(9):436–443.
43. Gyorffy B, Surowiak P, Budczies J, Lanczky A. Online survival analysis software to assess the prognostic value of biomarkers using transcriptomic data in non-small-cell lung cancer. *PLoS One*. 2013;8(12):e82241.
44. Kalluri R, Weinberg RA. The basics of epithelial-mesenchymal transition. *J Clin Invest*. 2009;119(6):1420–1428.
45. Lunt SJ, Chaudary N, Hill RP. The tumor microenvironment and metastatic disease. *Clin Exp Metastasis*. 2009;26(1):19–34.
46. Desgrosellier JS, Cheresh DA. Integrins in cancer: biological implications and therapeutic opportunities. *Nat Rev Cancer*. 2010;10(1):9–22.
47. Guadamillas MC, Cerezo A, Del Pozo MA. Overcoming anoikis — pathways to anchorage-independent growth in cancer. *J Cell Sci*. 2011;124(pt 19):3189–3197.
48. Giannoni E, et al. Redox regulation of anoikis: reactive oxygen species as essential mediators of cell survival. *Cell Death Differ*. 2008;15(5):867–878.
49. Giannoni E, Fiaschi T, Ramponi G, Chiarugi P. Redox regulation of anoikis resistance of metastatic prostate cancer cells: key role for Src and EGFR-mediated pro-survival signals. *Oncogene*. 2009;28(20):2074–2086.
50. Denoyelle C, et al. Anti-oncogenic role of the endoplasmic reticulum differentially activated by mutations in the MAPK pathway. *Nat Cell Biol*. 2006;8(10):1053–1063.
51. Croft A, et al. Oncogenic activation of MEK/ERK primes melanoma cells for adaptation to endoplasmic reticulum stress. *J Invest Dermatol*. 2014;134(2):488–497.
52. Nowis D, et al. Heme oxygenase-1 protects tumor cells against photodynamic therapy-mediated cytotoxicity. *Oncogene*. 2006;25(24):3365–3374.
53. Berberat PO, et al. Inhibition of heme oxygenase-1 increases responsiveness of pancreatic cancer cells to anticancer treatment. *Clin Cancer Res*. 2005;11(10):3790–3798.
54. Lee PJ, et al. Hypoxia-inducible factor-1 mediates transcriptional activation of the heme oxygenase-1 gene in response to hypoxia. *J Biol Chem*. 1997;272(9):5375–5381.

55. Was H, et al. Overexpression of heme oxygenase-1 in murine melanoma: increased proliferation and viability of tumor cells, decreased survival of mice. *Am J Pathol*. 2006;169(6):2181–2198.
56. Sunamura M, et al. Heme oxygenase-1 accelerates tumor angiogenesis of human pancreatic cancer. *Angiogenesis*. 2003;6(1):15–24.
57. Liu PL, et al. Resveratrol inhibits human lung adenocarcinoma cell metastasis by suppressing heme oxygenase 1-mediated nuclear factor-kappaB pathway and subsequently downregulating expression of matrix metalloproteinases. *Mol Nutr Food Res*. 2010;54(suppl 2):S196–S204.
58. Vigneswaran N, Wu J, Sacks P, Gilcrease M, Zacharias W. Microarray gene expression profiling of cell lines from primary and metastatic tongue squamous cell carcinoma: possible insights from emerging technology. *J Oral Pathol Med*. 2005;34(2):77–86.
59. Kobayashi T, et al. Thymosin-beta4 regulates motility and metastasis of malignant mouse fibrosarcoma cells. *Am J Pathol*. 2002;160(3):869–882.
60. Lokeshwar VB, et al. Urinary hyaluronic acid and hyaluronidase: markers for bladder cancer detection and evaluation of grade. *J Urol*. 2000;163(1):348–356.
61. Cisowski J, Loboda A, Jozkowicz A, Chen S, Agarwal A, Dulak J. Role of heme oxygenase-1 in hydrogen peroxide-induced VEGF synthesis: effect of HO-1 knockout. *Biochem Biophys Res Commun*. 2005;326(3):670–676.
62. Jozkowicz A, Was H, Dulak J. Heme oxygenase-1 in tumors: is it a false friend? *Antioxid Redox Signal*. 2007;9(12):2099–2117.
63. Sahoo SK, et al. Pegylated zinc protoporphyrin: a water-soluble heme oxygenase inhibitor with tumor-targeting capacity. *Bioconjug Chem*. 2002;13(5):1031–1038.
64. Carchman EH, Rao J, Loughran PA, Rosengart MR, Zuckerbraun BS. Heme oxygenase-1-mediated autophagy protects against hepatocyte cell death and hepatic injury from infection/sepsis in mice. *Hepatology*. 2011;53(6):2053–2062.
65. Banerjee P, et al. Heme oxygenase-1 promotes survival of renal cancer cells through modulation of apoptosis- and autophagy-regulating molecules. *J Biol Chem*. 2012;287(38):32113–32123.
66. Cairns RA, Harris IS, Mak TW. Regulation of cancer cell metabolism. *Nat Rev Cancer*. 2011;11(2):85–95.
67. Ron D, Walter P. Signal integration in the endoplasmic reticulum unfolded protein response. *Nat Rev Mol Cell Biol*. 2007;8(7):519–529.
68. Hetz C. The unfolded protein response: controlling cell fate decisions under ER stress and beyond. *Nat Rev Mol Cell Biol*. 2012;13(2):89–102.
69. Sayers CM, et al. Identification and characterization of a potent activator of p53-independent cellular senescence via a small molecule screen for modifiers of the integrated stress response. *Mol Pharmacol*. 2013;83(3):594–604.
70. Teske BF, et al. The eIF2 kinase PERK and the integrated stress response facilitate activation of ATF6 during endoplasmic reticulum stress. *Mol Biol Cell*. 2011;22(22):4390–4405.